Article

Early Alzheimer's Disease with frequent neuritic plaques harbors neocortical tau seeds distinct from primary age-related tauopathy

Danielle F. Browne [1,6], Denis S. Smirnov[2,3,6], David G. Coughlin [2], Iris Peng[1], Heidi G. Standke[1], Yongya Kim[2], Donald P. Pizzo[4], Alexandra Unapanta[4], Thea Andreasson[2], Annie Hiniker [4,5] ✉ & Allison Kraus [1] ✉

Tau neurofibrillary tangles (NFTs) in the presence of amyloid-β (Aβ) plaques are required for the diagnosis of Alzheimer's Disease (AD) and closely track with cognitive impairment, yet cognitively normal aged individuals frequently exhibit NFTs arising from tau seed accumulation. This may suggest that not all tau species are equally pathogenic and raises the question of whether unidentified tau modifications augment tau seeding activity and neurodegeneration in AD. We investigated how biochemical modifications of tau relate to clinicopathological outcomes in a cohort of 38 patients with Braak-matched AD neuropathologic change (ADNC) or primary age-related tauopathy (PART), a 3R/4R tauopathy with identical tau filament core structure to ADNC but with little to no Aβ deposition. We comprehensively measured tau histologic density, seeding activity using real-time quaking induced conversion (RT-QuIC) seed amplification assays, and select post-translational modifications (PTMs) (i.e. pT217, pS202/T205, & C-terminal epitopes) in hippocampus and neocortex. Even in cases without overt neocortical tau neuropathology, substantial hippocampal and neocortical tau seeding occurred in both PART and ADNC and predicted region-specific cognitive performance and longitudinal decline. Notably, tau seeding and PTM profiles were associated with Aβ neuritic plaque density and differentiated ADNC from PART in neocortex. Our data indicate that tau seed modifications meaningfully relate to disease trajectory, potentially explaining the more severe cognitive dysfunction observed in late-stage AD versus PART.

Tau neurofibrillary tangles (NFTs) are a highly prevalent neuropathology in aged individuals, with pre-tangle pathology nearly universal in individuals over age 40, tau-PET positivity in 100% of individuals over age 85, and frank histologic NFTs observed in all individuals by age 81 +[1,2]. Tau pathology in progressive Alzheimer's Disease (AD) is characterized by stereotyped regional accumulation of NFTs visible by histology[2,3], leading to the prevailing hypothesis that tau pathology can spread intercellularly throughout the brain. This pathological spread has been posited to occur directly through the intercellular transfer and protein-based propagation of misfolded tau

itself (whereby tau 'seeds' can recruit natively folded monomers to self-propagate filamentous structures), or through anatomically connected cellular spread of pathological processes that leads to tau post-translational modification, misfolding, and resultant toxicity[4,5]. Understanding the mechanisms that enhance tau misfolding and NFT accumulation is critical as it underlies the characteristic neuropathology and clinical presentation of tauopathies including AD.

NFT neuropathology that follows traditional Braak tau staging and occurs in the context of amyloid-β (Aβ) neuropathology is defined as AD neuropathologic change (ADNC). These AD-type tau NFTs have a characteristic 3R/4R isoform content and core filament structure[6]. However, even in the absence of Aβ deposition, tau NFTs with AD-type isoform content and structure can be found in a neuroanatomic distribution nearly identical to early ADNC, a neuropathology recently designated as primary age-related tauopathy (PART)[7–9]. PART is common, especially amongst the oldest individuals, with population estimates ranging from 20% of a Finnish population-based study of those aged 85 +[10] to over 40% of patients in *The 90+ Study of Aging*[11]. Though PART neuropathology involves the same neuroanatomic regions as ADNC in early Braak stages (I-IV), exceedingly few PART cases demonstrate the substantial neocortical tau pathology that is the hallmark of late-stage ADNC at Braak stages V and VI[12]. Neocortical AD-type tau is remarkably rare in the absence of Aβ deposition while medial temporal lobe tau in the absence of Aβ is quite common[12]. Thus, while the "amyloid cascade" hypothesis proposes NFT pathology in ADNC to be a downstream consequence of Aβ accumulation, the prevalence of PART in the population implies that an Aβ-independent mechanism of AD-type NFT formation is possible, at least within a limited neuroanatomic scope.

Multiple early studies reported that ADNC is associated with greater clinical impairment and more rapid cognitive decline than PART[13–15]. However, these studies generally compared high ADNC cases with extensive cortical tau pathology (Braak V-VI) to PART (definitionally Braak ≤IV)[13,14,16,17]. In contrast, we recently demonstrated that a cohort of PART cases with detailed cognitive testing showed no differences in clinical presentation, antemortem diagnosis, domain-specific cognitive impairment, or rates of longitudinal decline when compared to cases of Braak-stage matched (i.e. Braak I-IV) ADNC with comparable age at death[18]. Thus, parity in the rates of multiple measures of cognitive decline between PART and Braak I-IV ADNC suggests that the presence of neocortical Aβ deposits in ADNC but not PART does not lead to a meaningful clinical difference at early disease stages. Importantly, it remains unclear why and how PART and ADNC neuropathologies diverge in neocortical NFT accumulation and cognitive impairment later in disease presentation.

Ultrasensitive seed amplification assays such as real-time quaking-induced conversion (RT-QuIC) can be used to interrogate misfolded tau seeds, including those occurring prior to resultant NFTs[19]. RT-QuIC measures tau seeding activity as a readout of the capacity of amyloidogenic proteins to induce (seed) misfolding of natively folded monomer and can detect >billion-fold differences in biospecimen seeding activities[19,20]. Recent RT-QuIC and biosensor cell studies have suggested that (1) tau seeds are more neuroanatomically widespread than is captured by traditional IHC methods used for Braak staging and (2) tau seeds can occur well prior to overt neuropathology[19,21,22]. Further, these studies have indicated that tau from PART is capable of seeding[21,22], similar to tau from ADNC. However, whether PART and ADNC tau seeds are equivalent remains unclear. Mouse models with both Aβ and tau mutations demonstrate enhanced NFT accumulation, tau seeding, and neuropathology compared to mouse models harboring only tau mutations as detected by a phospho-tau antibody (AT8), the amyloid-specific dye Thioflavin S, and tau biosensor cell assays[23]. In contrast, tau biosensor cell readouts indicated there were no differences in tau seeding activities in ADNC versus PART across multiple brain regions in human cortical tissues (except for a possible

difference in the visual cortex at Braak IV)[22]. However, because few cases with both measurable neocortical tau seeding activity and Braak stages <IV have been examined, the extent to which Aβ neuropathology impacts early tau seeding in this region remains undefined.

The interplay between tau seeding activity and tau post-translational modifications (PTMs), and whether this differs between AD and PART is also unknown. Tau PTMs occur in the setting of AD and have been suggested to follow a semi-stereotyped temporal sequence with initial phosphorylation of tau's proline-rich region and C-terminal modification being detectable at the earliest Braak stages in ADNC[24]. Assays measuring these PTMs have been recently developed into CSF and plasma biomarkers for ADNC[25–27]. This evidence may indicate that additional structural modifications peripheral to the insoluble core structure of tau filaments could affect measurable tau seeding activity.

Here, we measured tau seeding activity in the hippocampus (HP) and middle frontal (MF) cortex of Braak-matched cases of ADNC and PART using a tau RT-QuIC assay[28] and compared tau seeding activity to the prevalence of select tau PTMs, tau density measured by digital histology, and the clinical and cognitive features of these cases. We hypothesized that differences in neocortical tau seeding activity detectable by RT-QuIC may discriminate patients with early ADNC from those with PART even in the absence of visible NFT deposition in the neocortex. We found that region-specific seeding activity can be detected in both ADNC and PART prior to the development of overt histologic neuropathology, and this seeding correlated with patients' global and region-specific cognitive performance and longitudinal decline. Specific PTM profiles were associated with increased neocortical tau seeding activity in matched early-Braak ADNC versus PART tissue, and also with increasing neuritic Aβ plaque density. Our findings provide a link between neocortical neuritic plaques, tau post-translational modification and seeding, and the distinct clinicopathological trajectories of ADNC and PART.

Results

Pathologic & clinical features are similar in ADNC & PART
PART and ADNC participants were well-matched in demographic, clinical, and neuropathologic features. On standard neuropathologic evaluation, they differed only in severity of Aβ neuropathology, which defined the groups (Thal phase 3-5 in ADNC, Thal phase 0-2 in PART, Table 1, Methods). For this study, the cohort was limited to Braak stage II through IV, and, importantly, the two groups were well-matched on Braak stage, suggesting similar neuroanatomic distributions of tau NFT pathology (Fig. 1a, Table 1). PART and ADNC groups also did not differ in age at death, the interval from last cognitive evaluation to death, or years of formal education (Table 1). As expected, the Alzheimer's risk factor, the *APOE* ε4 allele, was more common in ADNC than PART (Table 1). The two groups were cognitively similar overall on measures of global cognition, with comparable Mini-Mental State Exam (MMSE), Dementia Rating Scale (DRS), or Clinical Dementia Rating sum of boxes scores (CDR-sob, Table 1), and comparable rates of longitudinal MMSE decline in the years leading up to death (Table 1).

Tau digital histology does not differentiate PART & ADNC
In addition to Braak stage, which describes the neuroanatomic *distribution* of tau pathology, we quantitatively compared the precise histologic area occupied by tau pathology in PART and ADNC using digital histologic analysis of phospho-tau (AT8: pS202/pT205) IHC (Fig. 1b), measured in ln % area occupied (ln%AO). pS202/pT205 tau area occupied did not differ between HP in PART (from hereon designated "HP-PART") versus ADNC cases ("HP-ADNC") (Fig. 1c, Supplementary Table 1). pS202/pT205 tau area occupied also did not differ in the midfrontal (MF) cortex in PART ("MF-PART") versus ADNC ("MF-ADNC") (Fig. 1c, Supplementary Table 1). Thus, the two groups were matched on both neuroanatomical distribution of tau pathology and area occupied by tau neuropathology in both MF and HP. There

Table 1 | PART and ADNC cohorts demonstrate comparable demographic, clinical, and neuropathologic characteristics

	ADNC	PART	P value
n	21	17	
Age at Death	88.6 ± 8.9	89.6 ± 8.5	0.72
Female Sex	11 (52%)	7 (41%)	0.72
Hispanic/Latino Ethnicity	3 (14.3%)	3 (17.6%)	1.0
Thal Phase: 0 / 1-2 / 3 / 4-5	0 / 0 / 2 / 19 (0% / 0% / 10% / 90%)	9 / 8 / 0 / 0 (53% / 47% / 0% / 0%)	Definition
Braak Stage: II / III / IV	9 / 6 / 6 (43% / 29% / 29%)	7 / 4 / 6 (41% / 24% / 35%)	0.89
Neur Plaques: None / Sparse / Moderate / Frequent	0 / 2 / 13 / 6 (0% / 10% / 62% / 29%)	12 / 4 / 1 / 0 (71% / 24% / 6% / 0%)	2.4 x 10⁻⁶
LATE-NC: None / Amygdala / Hippocampus / Neocortex	14 / 1 / 3 / 1 (74% / 5% / 16% / 5%)	12 / 1 / 4 / 0 (71% / 6% / 24% / 0%)	0.91
Hippocampal Sclerosis	7 (33%)	3 (18%)	0.46
Age at Last Visit	87.8 ± 8.8	87.8 ± 8.1	0.95
Last Visit-Death Interval	0.8 ± 0.7	1.8 ± 2.6	0.16
Education	13.2 ± 5.1	14.9 ± 3	0.23
APOE e4 alleles: 0 / 1 / 2	10 / 9 / 2 (48% / 43% / 10%)	16 / 1 / 0 (94% / 6% / 0)	0.009
Clinical Diagnosis: Normal Cognition / MCI / Dementia	5 / 3 / 12 (24% / 14% / 57%)	8 / 0 / 9 (47% / 0% / 53%)	0.14
Last MMSE (/30)	20.9 ± 7.8	23.4 ± 8.7	0.38
Last DRS (/144)	116.1 ± 21.2	121.4 ± 22.5	0.47
Last CDR-sob (/18)	8.3 ± 7	7.1 ± 7.2	0.62
Rate of MMSE decline (points/year)*	-0.88 ± 0.22	-0.65 ± 0.26	0.50

LATE-NC Limbic Age-Related TDP-43 Encephalopathy - Neuropathologic Change, *APOE* Apolipoprotein E, *MCI* Mild Cognitive Impairment, *MMSE* Mini Mental State Exam, *DRS* Dementia Rating Scale, *CDR-sob* Clinical Dementia Rating - sum of boxes.
Missing data: LATE-NC ($n = 1$), last MMSE ($n = 1$), last DRS ($n = 1$), last CDR-sob ($n = 4$).
* Longitudinal decline estimates are group averages, at the mean values of covariates (age at death and years of education, as well as their interactions with time).
Statistics: Welch's unequal variance t-test for continuous variables, and Pearson's Chi-squared test (with Yates' continuity correction for 2x2 contingency tables), and linear mixed effects models for longitudinal decline. All statistical tests in this figure are two-sided, when applicable to the test type.

was no effect of sex on regional prevalence of tau neuropathology (Supplementary Table 2); sex had no significant impact on any of the other outcomes measured in this study (Supplementary Table 2).

Midfrontal tau seeding dose differentiates PART & ADNC
We next used endpoint dilution tau RT-QuIC analysis to estimate the regional tau seeding activity in brain homogenate (BH) for each PART and ADNC case (Fig. 1d). We previously showed that this technique can selectively identify 3R/4R tau seeding activity prior to neuropathological detection of tau via IHC[19,28]. Both HP-PART and HP-ADNC exhibited a range of 3R/4R seeding activities with indistinguishable distributions and means (Fig. 1e, Supplementary Table 1). In contrast, tau seeding activity was significantly elevated in MF-ADNC compared to MF-PART (Fig. 1e, Supplementary Table 1) despite low but comparable tau density in both MF-ADNC and MF-PART as measured by digital histology (above, Fig. 1c).

In prior work, we showed that, in MF-ADNC, tau seeding activity directly correlates with Braak stage, and occurs in substantial quantities even at low Braak stages lacking overt tau neuropathology[19]. We now examined the relationship between tau seeding activity in MF and

HP in our current cohort of ADNC and PART participants. In the ADNC group, MF seeding was positively associated with HP seeding (Fig. 1f), indicating that MF-ADNC seeding rises concordantly with HP-ADNC seeding. In contrast, in the PART cohort, MF seeding doses were consistently low and consequently did not increase with HP seeding doses (Fig. 1f). Importantly, our RT-QuIC findings reflect the known end-stage tau neuroanatomic distributions for ADNC and PART as measured by IHC but are measurable *prior* to significant NFT neuropathology, i.e. earlier in disease progression.

Tau seeding predicts domain-specific cognitive performance
Tau accumulation as measured by IHC and PET imaging correlates well with clinical cognitive impairment in ADNC[29–31]. It is not known if measures of tau seeding activity by RT-QuIC are clinically meaningful in the absence of significant regional IHC staining (for instance, when measured in the MF at low Braak stage). To investigate the clinical relevance of regional tau seeding activity, we examined the relationship between postmortem tau seeding doses and cognitive impairment during life over our entire study cohort of ADNC and PART participants (Fig. 2). We evaluated participant cognitive performance collected at the last cognitive evaluation before death and modeled rates of longitudinal decline across standardized annual cognitive evaluations in the 10 years preceding death. Performance was assessed with the MMSE as a global cognitive measure. Given our focus on HP and MF regions, blinded to seeding activity, we also generated memory and executive function cognitive domain composites from the extensive UCSD ADRC neuropsychological battery. Domain performance was then expressed as Z-scores normalized to the performance of cognitively normal ADRC participants who were not part of this study[18] (Fig. 2).

Both higher HP and MF seeding activities predicted lower MMSE scores at the evaluation nearest death (Fig. 2a). Importantly, when examining domain-specific cognitive measures, the memory composite outcome was only predicted by HP seeding activity, but not by MF seeding activity (Fig. 2b), while the executive function composite was predicted only by MF seeding activity, and not by HP seeding activity (Fig. 2c).

The same pattern emerged with longitudinal rates of decline. Higher HP and MF seeding activity predicted rates of longitudinal decline on the MMSE over the 10 years leading up to death (Fig. 2d). Memory decline was predicted only by HP but not MF seeding activity (Fig. 2e), while executive function decline was predicted only by MF and not by HP seeding activity (Fig. 2f). Together, these results indicate that regional tau seeding activities are related to region-specific cognitive impairment and longitudinal decline. The association of MF seeding with early stage executive dysfunction as well as its slow decline over time suggest that seeding activity measures a clinically meaningful process early in the disease course before overt pathology is observed by IHC in the MF.

The question arises if these cognitive associations are more related to group differences between ADNC and PART (or to the Aβ pathology which defines them), rather than to seeding activity itself. Mirroring the greater MF seeding activity seen in ADNC, there is a trend towards more impaired executive function ADNC patients compared to PART ($\beta \pm SE = -1.12 \pm 0.57$, $p = 0.06$), which may foreshadow further cognitive decline as ADNC patients accumulate more MF pathology at later disease stages (i.e., Braak V-VI). However, when either CERAD or Thal were included as covariates in the cognitive models of seeding used above, neither demonstrated an association with either memory or executive function (Supplementary Table 3). Rather, HP seeding remained a significant predictor of memory, while MF seeding remained a significant (or trend-level alongside CERAD) predictor of executive function (Supplementary Table 3). Overall, this suggests that tau seeding activity is a more direct correlate of these cognitive measures than CERAD or Thal, rather than a proxy for them.
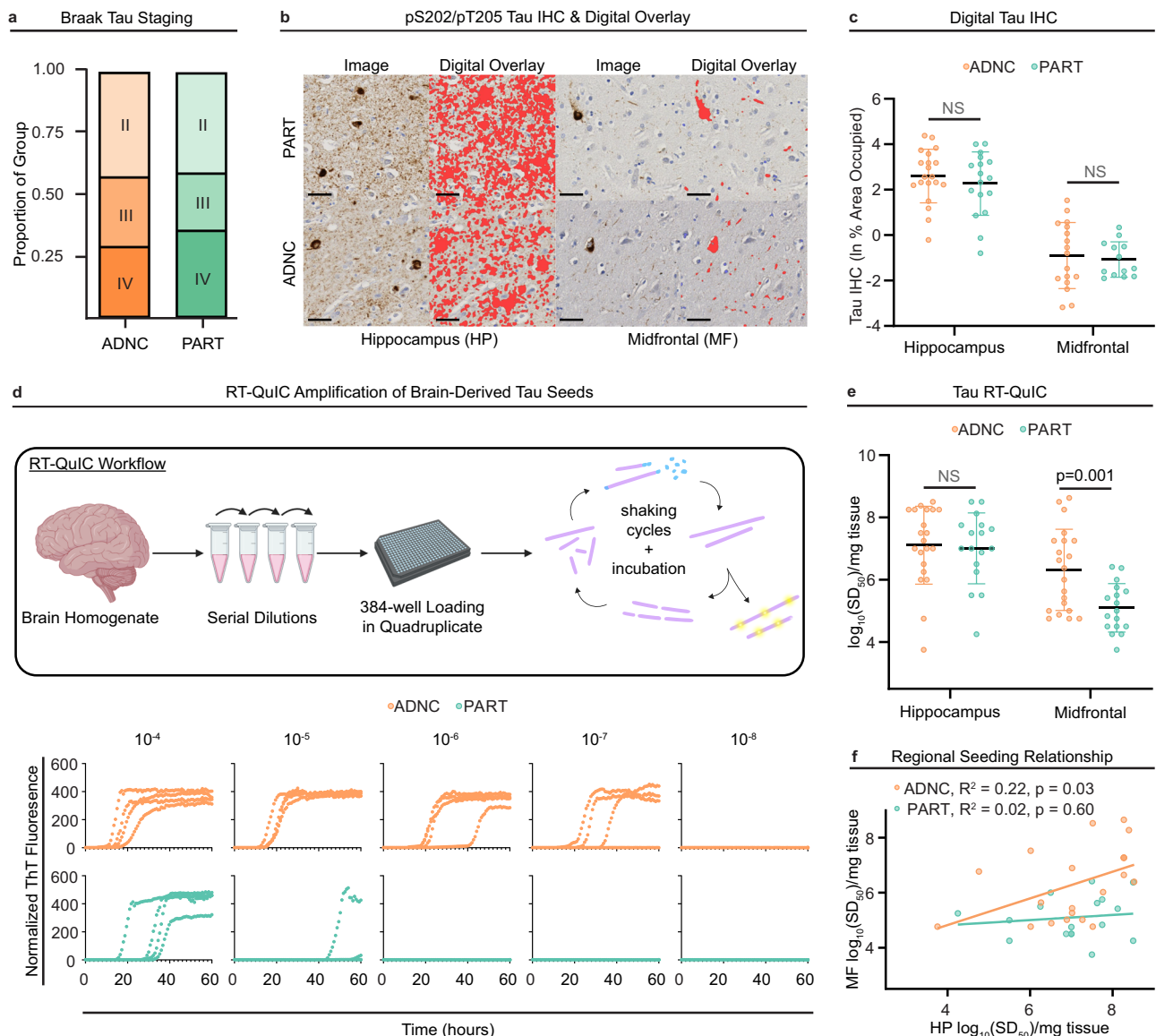
Fig. 1 | Higher 3R/4R tau seeding doses distinguish MF-ADNC from MF-PART.
a Alzheimer's Disease neuropathologic change (ADNC) and primary age-related tauopathy (PART) cases were Braak-matched across stages II-IV. The proportion of total ADNC (Braak II = 9, Braak III = 6, Braak IV = 6) and PART cases (Braak II = 7, Braak III = 4, Braak IV = 6) did not differ by group ($\chi2 = 0.23$, $p = 0.89$, Pearson's chi-squared test). **b** Digital histology was performed on hippocampal (HP) and mid-frontal (MF) tissues sections immunostained for pS202/pT205 tau. Representative images shown with digital overlay (red) indicate areas occupied. (Scale bars = 40μm). **c** Digital tau immunohistochemistry (IHC) quantitation (natural log of percent) of the image area occupied by tau staining showed comparable tau load between ADNC (HP $n = 20$, MF $n = 18$) and PART (HP $n = 17$, MF $n = 13$) across regions (p > 0.05, unequal variance t-test). Each data point represents a single quantification of the area occupied per participant. Center line represents the mean and the error bars represent the standard deviation for each group. **d** Endpoint dilution analysis of brain homogenate (BH) was performed with 3R/4R tau real-time quaking-induced conversion (RT-QuIC) assays in 384-well

microplates. Schematic[64] depicts seed amplification and fibril elongation (purple) with incubation and shaking cycles using Thioflavin T (ThT) fluorescence readouts (yellow). Data plots (bottom) show normalized ThT fluorescence readouts of quadruplicate well analysis across brain tissue homogenate dilutions ($10^{-4} - 10^{-8}$) for representative ADNC and PART cases. **e** Seeding doses [$\log_{10}(SD_{50})$/mg tissue] estimated from endpoint dilution analysis in HP and MF tissues showed increased 3R/4R tau seeding in MF-ADNC ($n = 21$) compared to MF-PART ($n = 17$) BH (unequal variances t-test). Seeding activities in HP tissues did not statistically differ (p > 0.05, unequal variance t-test). Each data point represents the average $\log_{10}SD_{50}$/mg brain tissue across 1-3 replicate endpoint dilution SD_{50} analyses of an individual case. The center line and error bars represent the mean and standard deviation of the participant-averaged data points. **f** ADNC but not PART cases exhibited a significant positive correlation between MF and HP seeding activities (Pearson's correlation). All statistical tests in this figure are two-sided, when applicable to the test type.

Midfrontal tau post-translational modifications differ between PART & ADNC

In an effort to define characteristics of tau seeds that drive differential MF-PART and MF-ADNC seeding activities, we investigated biochemical attributes prevalent in ADNC tau, specifically solubility and phosphorylation PTMs. We derived sarkosyl-insoluble (SI) tau from MF of both ADNC and PART to determine the degree to which tau seeds

share properties with the highly structured insoluble filaments comprising NFT neuropathology (Fig. 3a). A majority of tau seeding activity recovered from brain homogenate is retained in the SI fractions compared to the soluble fractions, suggesting that most of the seed-competent species in ADNC and PART are insoluble, even at early Braak stages (Fig. 3a, Supplementary Fig. 1a). Additionally, MF-ADNC SI fractions exhibit greater seeding activity than MF-PART SI fractions
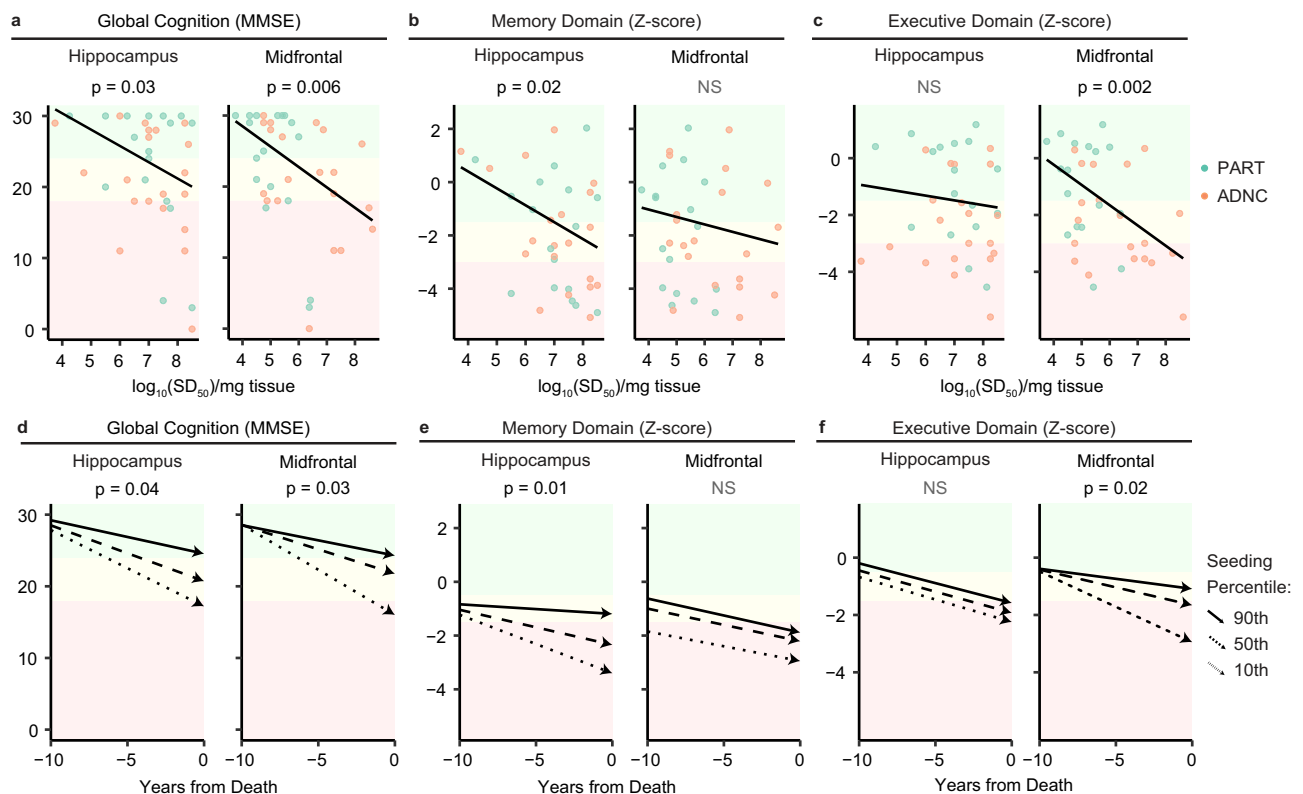
Fig. 2 | Tau seeding activity in brain homogenate (BH) correlates with global and region-specific cognition and longitudinal decline. a Performance on the Mini Mental State Exam (MMSE, a measure of global cognition) at the final cognitive evaluation prior to death ($n = 37$) was negatively associated with increasing seeding doses in the HP and MF regions (linear regression). **b**, **c** In contrast, Memory Domain composite scores (expressed as Z-scores relative to the performance of robust normal control participants) were associated only with HP seeding ($p = 0.02$, linear regression), while Executive Function scores correlated only with MF seeding ($p = 0.002$, linear regression). All regression models in **a**–**c** were adjusted for patient age and years of formal education. **d** Longitudinal cognitive analyses demonstrated a more rapid rate of decline on the MMSE in the 10 years leading up to death with increasing HP and MF seeding (mixed effects regression, plotted as trajectories at the 10th, 50th, and 90th seeding percentile). **e, f** As with the cross-sectional analysis above, the rate of Memory Domain decline was associated only with HP seeding, while Executive Function declined more rapidly only with increasing MF seeding (mixed effects regression). All longitudinal analyses in e-f were performed using linear mixed-effects models with random slopes and intercepts by the participant, as well as adjustment for patient age, education, final score, and each of these terms' interaction with time (measured as years from death). All statistical tests in this figure are two-sided.

(Supplementary Fig. 1b), similar to the observation made in BH (Fig. 1e). The amount of SI material derived from each respective tissue did not significantly differ by diagnosis or by MF or HP region, nor did it correlate with measures of seeding activity or digital histology, suggesting this is not a driver of the observed differences (Supplementary Fig. 2).

We then examined brain homogenate (BH) and SI tau by immunoblot for multiple tau epitopes, including a phospho-tau marker classically used for Braak staging (pS202/pT205), an emerging phospho-tau biomarker (pT217), and a C-terminal tau epitope (region around D430) that has been described to be enriched in AD cases[32] (Fig. 3b). We noted a striking increase in immunoreactivity of all three epitopes in a representative sampling of our MF-ADNC (Braak II-IV) cases as well as in positive control MF-high ADNC (Braak V/VI) cases (details of the positive control Braak V/VI group in Supplementary Table 4) when compared to equivalent amounts of brain tissue from select Braak II-IV MF-PART cases (Fig. 3c). pS202/pT205 and pT217 tau immunoreactivity were largely absent from both the total BH and the SI fraction of MF-PART, and C-terminal tau immunoreactivity was strikingly reduced compared to MF-ADNC (Fig. 3c).

Based on these observations, we completed dot immunoblots on BH from all 38 cases in our cohort, staining for pS202/pT205, pT217, and C-terminal tau in both MF and HP regions (Fig. 3d) and normalizing to a total protein stain. Immunoreactivity was increased in MF-ADNC compared to MF-PART for all three epitopes namely (pS202/

pT205)/total protein, pT217/total protein, and C-terminal tau/total protein (Fig. 3e–g). In contrast, although average pS202/pT205, pT217, and C-terminal tau immunoreactivity were higher in HP than MF in both groups, there were comparable levels of each of these epitopes in HP-PART and HP-ADNC (Fig. 3e–g). Together, this suggests that while these tau PTMs are found at similar levels in both HP-PART and HP-ADNC, they are much less abundant in MF-PART than MF-ADNC, recapitulating the pattern observed in seeding activities (Fig. 1e).

Our results suggest potential for two distinct possibilities: either increased tau seeding activities reflect more tau seeds in MF-ADNC compared to MF-PART and the proportion of PTMs per tau seeding unit is equal (i.e., a *quantitative* difference in tau seeds), or there are equivalent amounts of tau seeds in MF-ADNC compared to MF-PART but the seeds themselves are differentially modified (i.e., a *qualitative* difference in tau seeds). These possibilities are not mutually exclusive, and a combination thereof would also contribute to increased overall seeding activities in MF-ADNC. We therefore normalized PTMs to total tau. We evaluated immunoblots using two mid-domain tau antibodies routinely used to approximate total tau, BT2 and HT7 (Supplementary Fig. 3a). HT7 targets aa159-163 while BT2 targets aa194-198; both have been extensively used in immunoblotting to measure total tau from human brain tissue[33]. However, there was little concordance in staining patterns between these two antibodies, especially in SI fractions, suggesting they may be marking different tau species (Supplementary
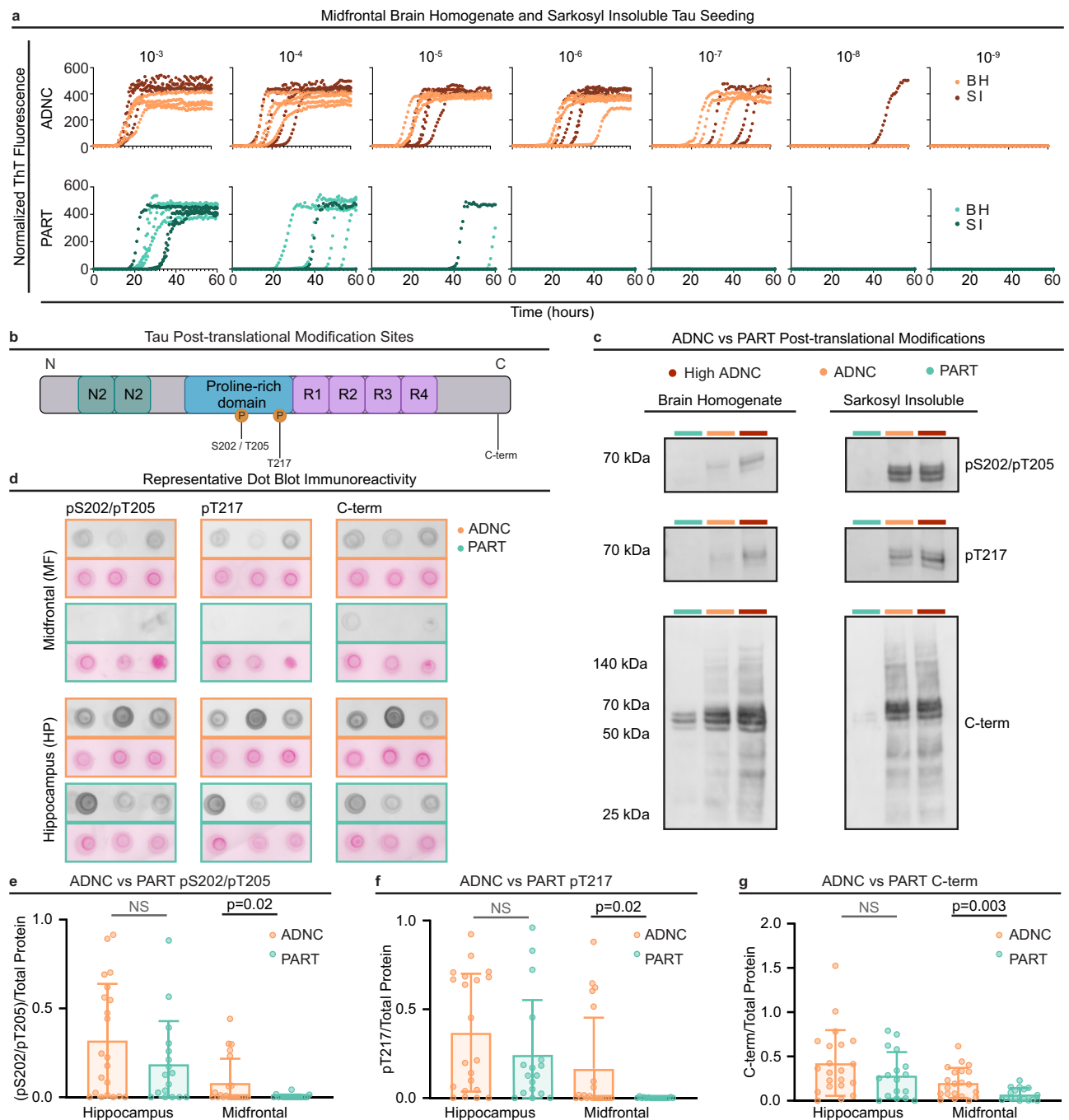
Fig. 3 | Sarkosyl-insoluble (SI) fractions and brain homogenate (BH) exhibit increased tau PTMs in MF-ADNC compared to MF-PART. a Representative seeding activity endpoint analysis of MF-ADNC and MF-PART brain homogenates (BH) and BH equivalents of sarkosyl-insoluble (SI) extracts. Normalized Thioflavin T (ThT) fluorescence readouts of indicate seed amplification of 10^{-3}-10^{-9} BH and SI dilutions. **b** Schematic of select tau post-translational modifications (PTMs) investigated and their relative location on tau primary structure. Regions used to characterize the tau sequence are included: N-terminal inserts (green), proline-rich domain (blue), and microtubule binding repeats (purple). Phosphorylation events are marked at S202/T205 and T217. The C-terminal (C-term) region of interest is marked near D430. **c** Western blots representing MF-PART, MF-ADNC, and MF-high ADNC (Braak VI) pS202/pT205, pT217, and C-terminal immunoreactivity in BH (5%

w/v) and SI extracts (0.1 mg/ml). Similar results have been obtained across 3+ technical replicates. **d** Representative BH (5% w/v) dot blot pS202/pT205, pT217, and C-terminal immunoreactivity (greyscale) of 3 cases of both HP and MF regions of ADNC and PART and total protein staining (Ponceau S, pink). **e**–**g** Quantitation of BH dot blot immunoreactivity relative to total protein staining in HP and MF regions of all ADNC ($n = 21$) and PART ($n = 17$) cases. Each point represents the average of an individual case across 3 replicates, bars represent the group means, and error bars represent standard deviations across the averaged replicate values. MF-ADNC cases had significantly higher immunoreactivity compared to MF-PART cases for each pS202/pT205, pT217, and C-terminal antibodies (unequal variance t-test). In contrast, HP-ADNC and HP-PART did not differ across these epitopes ($p > 0.05$, unequal variance t-test). All statistical tests in this figure are two-sided.

Fig. 3b). Comparison of total HT7 and BT2-reactive tau between our ADNC and PART groups suggested there may be a decreased amount of tau marked by these antibodies in the MF of the PART group (Supplementary Fig. 4a, b). Nonetheless, the results obtained when pS202/pT205, pT217, and C-terminal immunoreactivity were normalized to total protein and either of the total tau antibodies (BT2 and HT7) (Supplementary Fig. 4c, d) were consistent with results normalizing to total protein alone (necessary for interblot comparison) and

demonstrated decreased PTMs per unit tau in MF-PART compared to MF-ADNC. Together, this supported the existence of a *qualitative* difference in the tau species present in the neocortex of ADNC vs PART.

Tau seeding and post-translational modifications are independent of APOE genotype

It has been well-established that ADNC and PART have differing apolipoprotein E (*APOE*) genotype frequencies. *APOE* ε4 is less common in PART but more common in ADNC, and the ε4 allele is associated with increased Aβ deposition relative to ε3 or ε2 allele[34]. This finding is recapitulated in our cohort, in which only 1 of 17 PART participants (6%) harbored a single *APOE* ε4 risk allele, while 11 of 21 ADNC participants (52%) harbored at least a single ε4 allele (and two patients were homozygous ε4/ε4), raising the possibility that the group differences in neocortical tau seeding and PTMs could be related to this disparity (Table 1).

To assess this possibility, we compared the results from univariate regression models of tau seeding/PTMs by group to models that included a term for the presence of the *APOE* ε4 risk allele (Supplementary Table 5). When the APOE ε4 allele term is added to the models, the same relationships remain significant, while the ε4 term itself never reaches significance.

Since the *APOE ε4* allele is present in 52% (approximately half) of our ADNC participants, this cohort is useful to directly test the effect of *APOE ε4* on tau seeding and PTMs without the confounding factor of diagnostic group. We find no difference in MF seeding or MF tau modifications between the ADNC cohort with ε4 and the ADNC cohort without an ε4 allele (Supplementary Fig. 5). Overall, these findings imply that *APOE ε4* genotype is a risk factor for the development of Aβ pathology (and in turn ADNC, both of which are well established) but that *APOE ε4* is not in itself the main driver of tau PTMs and seeding results.

Tau seeding in midfrontal cortex relates to neuritic plaque density

Our results thus far showed greater tau seeding activity and PTMs in MF-ADNC than MF-PART (irrespective of *APOE* status) and showed that tau seeding in both MF and HP correlated with domain-specific cognitive dysfunction. These observations suggested that there may be a factor(s) augmenting select MF tau PTMs and seeding activity in ADNC compared to PART. A hallmark of ADNC is significant Aβ neuropathology in MF even at early Braak stages. We therefore hypothesized that Aβ neuropathology in MF could directly or indirectly modify tau seeds to influence seeding activity. To test this, we examined the relationship between regional tau seeding and measures of tau (Braak stage) and Aβ neuropathology (CERAD neocortical neuritic plaque density and Thal Phase Aβ plaque distribution), which form the basis of the neuropathological distinction between ADNC and PART.

While HP seeding was unrelated to either CERAD neuritic plaque density or Thal phase (Fig. 4a), MF seeding was significantly associated with CERAD density (F = 14.61, p < 0.001, ANOVA (type II)), and post-hoc analysis indicated that seeding was greater in those with a frequent neuritic plaque score compared to those with no, sparse, or moderate plaque density (Fig. 4a). Similarly, MF tau seeding was associated with Thal phase (F = 4.06, $p = 0.01$, ANOVA (type II)), with greater seeding in those with Thal phases 4-5 compared to those with Thal phase 0 (Fig. 4a). Finally, we examined seeding activity across Braak stages of tau pathology across the entire cohort (ADNC and PART), which showed increased HP seeding activity with higher Braak stage (F = 5.41, $p = 0.009$, ANOVA (type II)), with a significant post-hoc difference between those with Braak stage II versus IV. By contrast, MF seeding activity did not significantly differ over these early Braak stages (Fig. 4a).

An examination of this breakdown allowed comparison of patients that met criteria for "definite" PART (defined in our

study using the preferred criteria as those with Thal phase 0 (alternative criteria is CERAD 0) to those with "probable" PART (Thal 1-2 in our study, or alternatively CERAD 1), and demonstrated no significant differences between the two sub-categories of PART (Fig. 4a). Further, this analysis revealed that within ADNC, those with relatively more dense neuritic plaques (CERAD 3) had elevated tau seeding compared to those with relatively fewer plaques (CERAD 2). To establish if this effect was due to an association of higher CERAD scores with more advanced tau pathology, we repeated this analysis in exclusively intermediate ADNC patients (defined by Thal phase 3-5 and Braak stage III-IV), where there was a range of CERAD scores (CERAD1: $n = 1$, CERAD 2: $n = 5$, and CERAD 3: $n = 6$). Within this group of patients, MF seeding remained associated with increasing CERAD score (F = 8.4, $p = 0.02$), with a post-hoc difference between those with CERAD 3 versus 2 ($p = 0.03$).

Given that the ordinal CERAD neuritic plaque density and Thal Aβ phase appeared to demonstrate a consistent effect on cortical tau seeding, we sought to employ a more granular measure of Aβ density using digital quantification of %AO by Aβ IHC (as we had done previously with tau). The results indicate that within the entire cohort, there are significant correlations of HP seeding activity separately with both HP tau and HP Aβ histologic digital area occupied, but when controlling for both in a two-way ANOVA, tau burden drove the seeding association while the Aβ digital area occupied term was not significant (Supplementary Table 6). In the MF, there were only trend-level associations of MF seeding activity separately with both Aβ and tau histologic frequency (acknowledging that this is scant in Braak II-IV cases). In multivariable models, these analyses remained trend level for both tau and Aβ (Supplementary Table 6). We note that this digital histologic assessment captures the area occupied by any Aβ immunoreactivity, rather than the density only of neuritic plaques as is measured by CERAD. This could suggest that neuritic plaques specifically play a distinct role in this relationship, in line with the stronger association of MF seeding with CERAD compared to Thal phase.

Tau seed post-translational modifications correspond with higher neuritic plaque density

While select tau PTMs were associated with MF tau in ADNC (but not PART) there was a range of pS202/pT205, pT217, and C-terminal tau immunoreactivity. Thus, we examined the relationship of tau seed PTMs with CERAD density in MF from Braak stage IV cases with different CERAD scores using immunoblot of both representative BH and SI fractions. Increased phospho-tau and C-terminal immunoreactivity corresponded with higher Aβ neuritic plaque density (Fig. 4b). By contrast, IHC demonstrated comparable pS202/pT205 tau staining despite differences in the density of neuritic plaques in MF regions (Fig. 4c). Similar to seeding activity, MF (but not HP) CERAD neuritic plaque *density* was associated with greater tau phosphorylation at pS202/pT205, pT217, and with increased C-terminal immunoreactivity (Fig. 4d–f). Thal phase was associated only with greater C-terminal immunoreactivity, while Braak stage was not associated with any of these epitopes in MF (Supplementary Fig. 6). These observations may suggest a facilitative role of neuritic plaque related processes in tau PTMs. It should also be noted that this effect was not observed in HP (Supplementary Fig. 7), consistent with a possible region-dependent influence of Aβ neuritic plaques.

Post-translational modifications mark tau seeds with higher seeding activities

Given that both MF tau seeding activities and PTMs independently correlated with increased Aβ neuritic plaque density, we compared immunoreactivity with seeding activity in all cases. MF-ADNC cases with more PTMs exhibited higher seeding activity (Fig. 5a–c). Interestingly, these same select tau PTMs demonstrated a significant relationship with tau seeding activity in both HP-PART and HP-ADNC cases
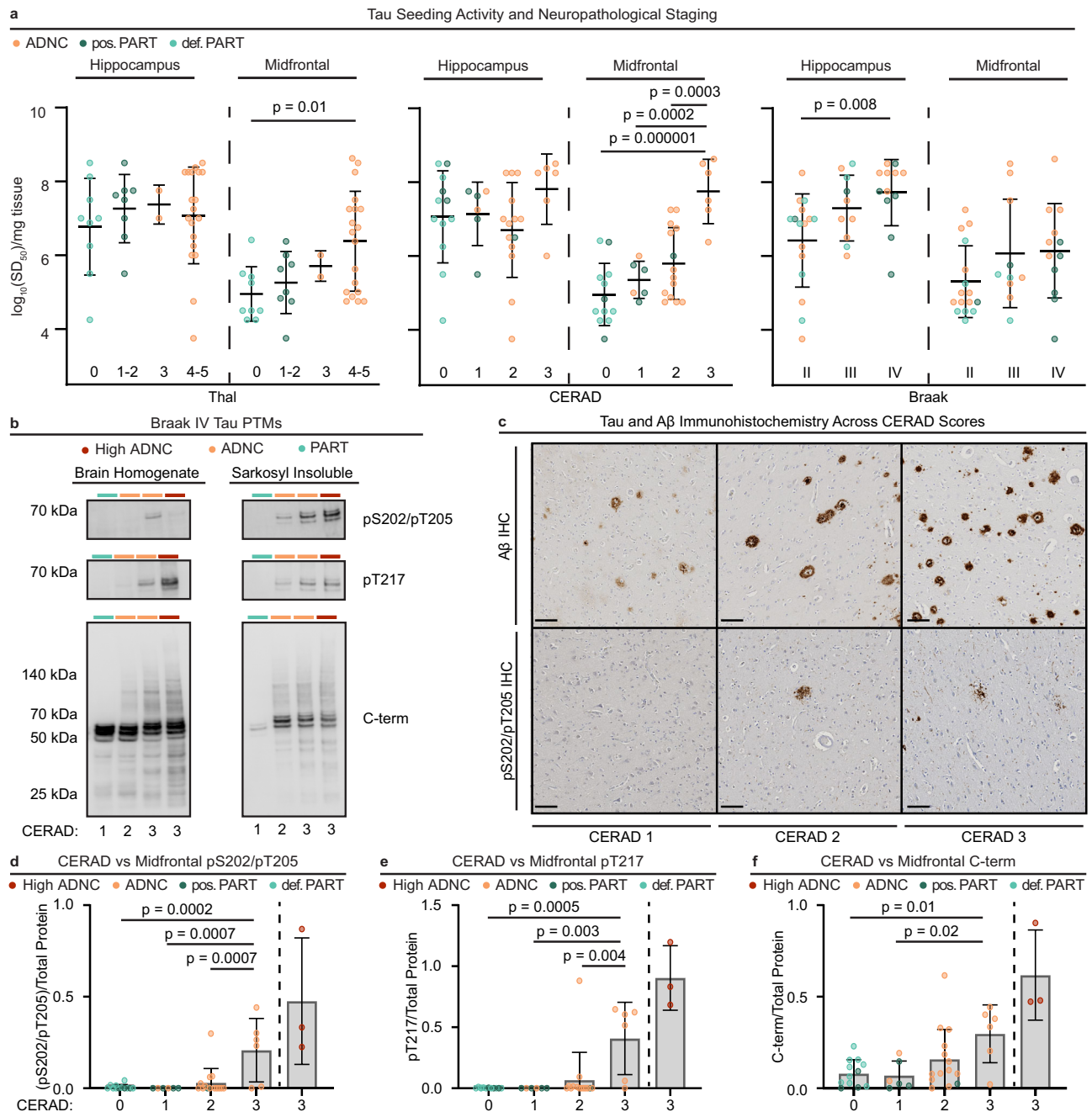
Fig. 4 | Amyloid-β neuritic plaque density correlates with increased MF-ADNC tau seeding activity and PTMs. a Tau brain homogenate (BH) $\log_{10}SD_{50}$s (average across 1-3 replicate endpoint dilution analyses) from all cases organized by neuropathological staging of tau (Braak stages, II: $n = 16$, III: $n = 10$, IV: $n = 12$) and Aβ (CERAD scores 0: $n = 12$, 1: $n = 6$, 2: $n = 14$, 3: $n = 6$ and Thal phases 0: $n = 9$, 1-2: $n = 8$, 3: $n = 2$, 4-5: $n = 19$). Center line represents mean, while error bars correspond to standard deviation. Statistical significance depicted corresponds to Tukey's Honest Significant Difference (HSD) test, employed as a post-hoc test when an overall ANOVA demonstrated significance differences for MF seeding by Thal phase ($F = 4.1$, $p = 0.01$) and CERAD score ($F = 14.6$, $p = 2.8 \times 10^{-6}$), as well as HP seeding by Braak stage ($F = 5.4$, $p = 0.009$). **b** Representative BH (5% w/v) and SI extract (0.1 mg/mL) tau PTM Western blots of Braak IV cases across CERAD scores 1-3. A high ADNC (Thal 5, Braak VI, CERAD 3) sample is included as a positive control. Similar results have been obtained across 3+ technical replicates. **c** Representative

pS202/pT205 tau and Aβ immunohistochemistry (IHC) staining (brown) of Braak IV cases across CERAD scores 1-3. (Scale bar = 100 μM). **d**–**f** Tau PTM immunoreactivities of MF BH normalized to total protein staining of individual cases (averages across 3 replicates) grouped by CERAD scores (0: $n = 12$, 1: $n = 6$, 2: $n = 14$, 3: $n = 6$). Bars represent group means and error bars are standard deviations across the averaged replicate values. A high ADNC group ($n = 3$) is included for comparison but was not included in statistical analyses (demographics detailed in Supplementary Table 1). Statistical significance depicted corresponds to Tukey's HSD test, employed as a post-hoc test when an overall ANOVA demonstrated significance differences for MF pS202/T205 ($F = 9.2$, $p = 1.3 \times 10^{-4}$), pT217 ($F = 7.4$, $p = 6.0 \times 10^{-4}$), and C-term ($F = 4.3$, $p = 0.01$). Possible (pos., $n = 8$) and definite (def., $n = 9$) PART subgroups are as indicated. All statistical tests in this figure are two-sided, when applicable to the test type.
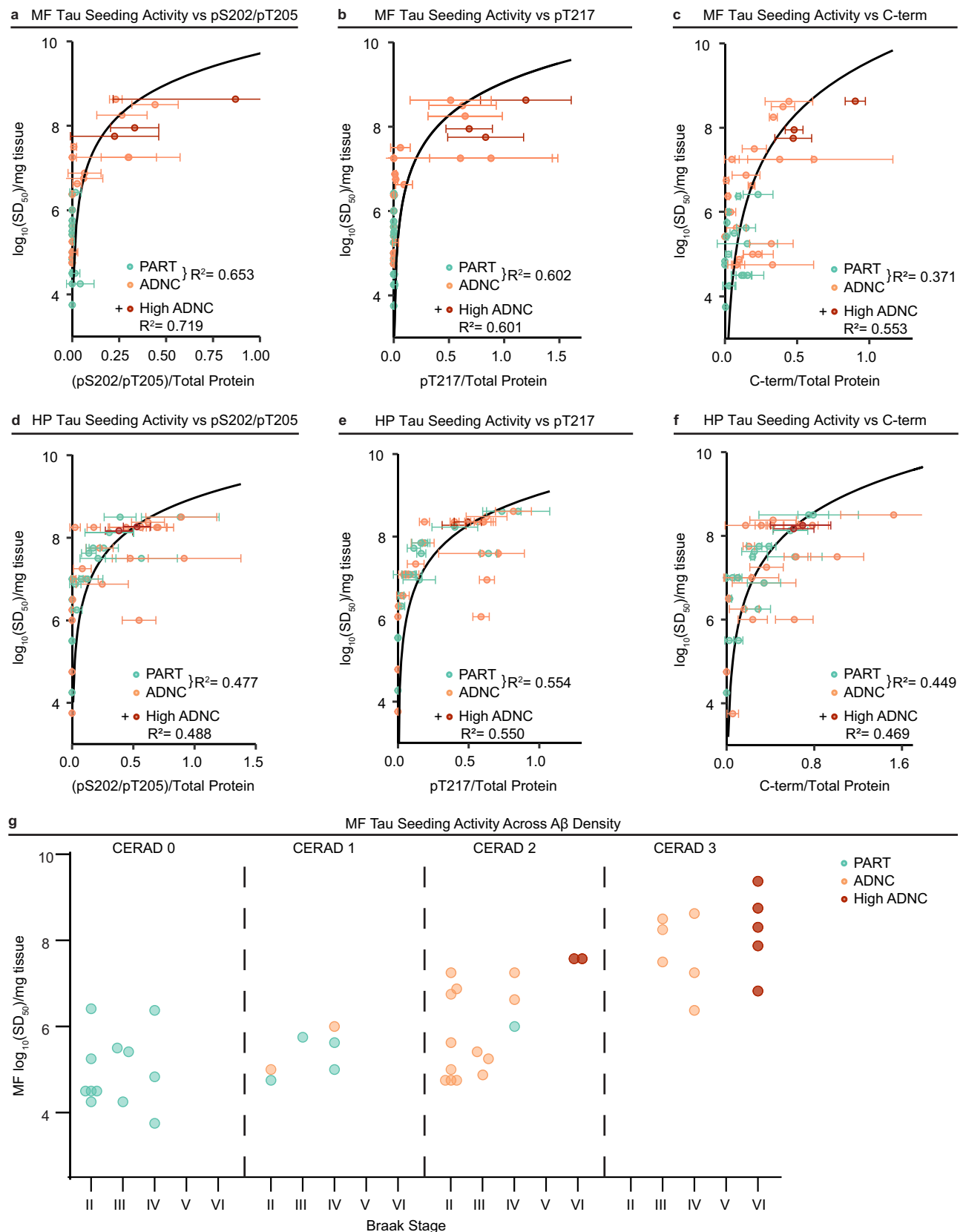
Fig. 5 | MF-ADNC cases with increased tau PTMs exhibit the highest seeding activities. Case-by-case correlation of MF **a**–**c** and HP **d**–**f** brain homogenate (BH) seeding doses and post-translational (PTM) immunoreactivities normalized to total protein staining. Each point represents a single case (ADNC $n = 21$, PART $n = 17$) with average immunoreactivity and standard deviation over 3 replicates and average $\log_{10}SD_{50}$ determinations (1-3 replicates). The logarithmic regression model fits the ADNC and PART cases and associated R^2 values are displayed. High ADNC cases (red, $n = 3$ for MF, $n = 2$ for HP, Supplementary Table 4) follow the same relationship, and R^2 values with their addition to the modeled cohort are also displayed. **g** Mapping of MF-ADNC ($n = 21$) and MF-PART ($n = 17$) BH $\log_{10}SD_{50}$s across Braak stage and CERAD scores. High ADNC (Braak VI, $n = 7$) samples are included for comparison. All statistical tests in this figure are two-sided.

(Fig. 5d–f). This further suggests synergy between PTMs and seeding that occurs regardless of brain region, with our evidence also indicating this may be augmented by neuritic plaque-related processes in a region-specific manner (Fig. 5g). Increased HT7 immunoreactivity had a more significant relationship with seeding activity than BT2 when normalized to total protein (Supplementary Fig. 8a, b), again suggesting that they may mark different tau species. Still, similar results were observed when the pS202/pT205, pT217, and C-terminal tau species were normalized to total protein and total tau (BT2 and HT7) (Supplementary Fig. 8c, d). Importantly, our results are consistent with a relationship between neuritic plaque density and accumulation of MF tau with specific disease-associated PTMs and increased tau seeding activity.

Discussion

PART and ADNC harbor identical 3R/4R tau core filament structures[9] yet exhibit distinct clinical progression and end-stage neuropathology. Here, we investigated the extent to which neuroanatomically defined tau seeding activity and PTMs peripheral to the insoluble core can elucidate discrete disease trajectories within a cohort of PART and ADNC cases. Using tau RT-QuIC[28] and immunoblotting assays, we found that 3R/4R tau seeding activity and PTM prevalence were increased specifically in the middle frontal cortex of cases of ADNC compared to Braak-matched PART with equivalent tau burden as measured by digital histology. Additionally, we observed that tau seeding predicted domain-specific cognitive impairment and longitudinal decline prior to overt NFT pathology detected by IHC.

Here we demonstrate that specific PTMs differentiate tau filaments with identical core structures, expanding the possible structural drivers of tau seeding activity. Increased tau seeding activity in ADNC versus PART neocortex is marked by not only increased tau phosphorylation at epitopes pS202/pT205 and pT217, but also increased immunodetection of an epitope at varying molecular weights in the extreme C-terminus near D430 (Figs. 3 and 4). AD-related proteolytic C-terminal truncation of tau has been suggested by others to occur at a cleavage site N-terminal to the D430-region epitope used here[24,27,35]. Interestingly, on denaturing gels, we observed increased C-terminal reactivity at molecular weights both higher and lower than that of full-length 3R or 4R tau isoforms, implying that truncation fragments, or potentially mixtures of truncated and non-truncated tau, may be cross-linked and contribute to this higher molecular weight immunoreactivity. Regardless, our results are consistent with prior immunolabeling with the same C-terminal antibody showing increased immunoreactivity in Braak V-VI ADNC cases[36]. Recent work by others showed that tau PTMs relate to increased tau seeding activity in AD[24]. Our work here complements this study by specifying structural modifications that appear to delineate PART and ADNC tau seeding activities.

Known AD-related tau PTMs include complex combinations of specific phosphorylation, acetylation, ubiquitination, and cleavage modifications, among others. Understanding the prevalence of these modifications necessitates standardization against a reliable total tau standard, which has historically included antibodies targeting mid-domain epitopes to capture all isoforms and cleavage fragments. In performing this study, we normalized all tau PTM measurements not only to total protein levels but also to two mid-domain tau antibodies frequently utilized to measure all tau isoforms or "total tau" (Figs. 3–5, Supplementary Figs. 4, 8). While our observation that specific PTMs per unit tau increases with neuritic plaque density as measured by CERAD score held true regardless of which total tau antibody was used for normalization, there was significant variation in the extent to which each total tau antibody recognized tau in BH and SI fractions (Supplementary Figs. 3, 4, 8). Prior observation of increased BT2 immunoreactivity upon alkaline phosphatase treatment is consistent with our observation here of reduced BT2 labeling of highly phosphorylated SI fractions[37]. In the absence of high-resolution information

about tau structural characteristics that occur outside of the highly ordered core, we suggest that there is utility in measuring total tau using antibodies targeting multiple tau epitopes. This will better inform more precise quantification of tau amount, particularly when attempting to distinguish PTMs on multimeric and fibrillar tau seed assemblies.

Specific tau fibril structures characterize neuropathologically distinct tauopathies, providing evidence for tau strains in neurodegenerative diseases[6]. The term "strain" derives from observations in the prion field that different misfolded protein conformations underpin discrete disease phenotypes[38], which were canonically defined by distinct clinical and neuropathological outcomes, and recently also distinguished by differences in prion fibril core structures[39-41]. Our findings here suggest that different PTMs distinguish clinicopathological outcomes, despite the presence of a conserved insoluble core structure. This raises important questions of how definitions of strain can fully encompass all structure-based information (such as PTMs) to relate to clinical outcomes. Recent findings suggest that some, but not all, PTM profiles from insoluble ex vivo seeds are reproduced in seeded cell models[42]. It is interesting to speculate that variation in the replication of PTMs in addition to replication of the fibril core structure could establish unique clinical presentations in specific biochemical and cellular contexts (e.g. when protein seeds such as Aβ and tau co-occur).

The presence of neocortical seeding activity in both ADNC and PART prior to overt NFTs suggests that not only AD-type but also PART-type tau seeds commonly occur in neocortex. Whether tau seeds isolated from MF in PART and ADNC at these early Braak stages (≤ IV) are derived from seeds that spread from the medial temporal lobe or from nucleation events within the neocortex remains unclear. It has been proposed that after Braak stage III, the local replication rate is the limiting factor of tau accumulation rather than the geographic spread; thus, the importance of these processes may differ depending on the disease stage[43]. Regarding our observed differences in MF-PART versus MF-ADNC seeding activities; we cannot rule out that collective fibril ultrastructure differences may also contribute (e.g. mixed composition of paired helical and straight filaments [both incorporating the shared amyloid core structure], mixed lengths, mixed fibril maturity at a given pathological stage, etc). Regardless, lower tau seeding activities in the PART neocortex is consistent with the rarity of Braak stage V PART cases[12]. We also hypothesize that certain PTM profiles on identical tau core structures could contribute to distinct clinicopathological outcomes. Further study is required to understand how the PTMs observed here facilitate (but are not required to initiate) misfolding pathways. These studies are particularly relevant to the kinetics of tau templating and monomer incorporation, as we predict PTMs can influence tau seed replication and/or spread.

Though tau seeds in ADNC and PART exhibit distinct PTMs, our identification of robust tau seeding in PART supports that Aβ neuropathology is not a necessary precursor of AD-like tau neuropathology as is proposed by the amyloid cascade hypothesis. However, our observations of increased tau seeding and PTMs in the neocortex of ADNC cases with frequent Aβ neuritic plaques compared to PART cases with similar tau burden by IHC, suggest that neuritic plaque-associated mechanism(s) may influence tau seeding activity in the neocortex (Fig. 6). It is important to note that increased tau seeding and modification is more significantly related to CERAD score, which specifically reflects neuritic plaque density, than to Thal phase, which reflects the neuroanatomic location of Aβ pathology visible on IHC regardless of type. Although our study does not demonstrate the directionality of this relationship or identify whether intermediary mechanisms are involved, it is interesting to note that there is a direct accumulation of tau fibrils in Aβ neuritic plaques[44]. These specific accumulations are thought to indicate upregulated neuroinflammatory processes, perhaps implying that Aβ augments tau post-
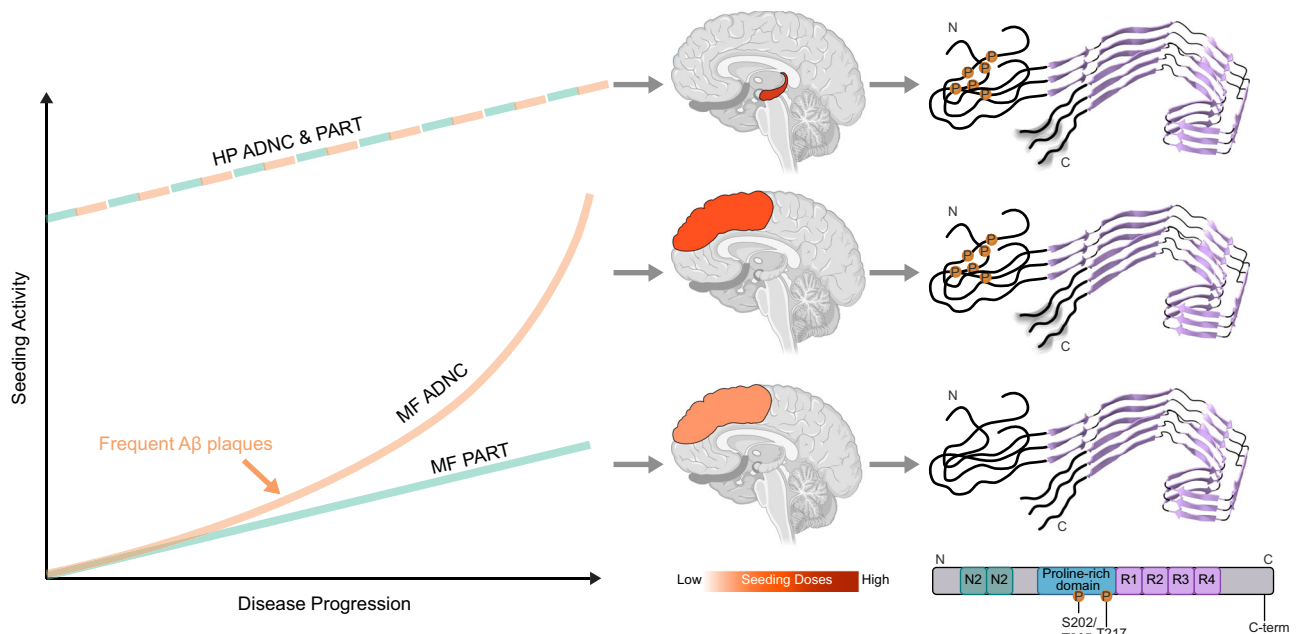
Fig. 6 | Tau seeding and select post-translational modifications (PTMs) associate with Aβ neuritic plaque density and differentiate Alzheimer's Disease neuropathologic change (ADNC) from primary age-related tauopathy (PART). Graphical depiction summarizing comprehensive measurements of tau seeding activity and select PTMs (i.e. pS202/pT205, pT217, and C-terminus) in hippocampus and neocortex. Tau seeding in hippocampus (HP) and midfrontal cortex (MF) increases with disease progression and overall tau NFT Braak stage in ADNC and PART cases. However, Aβ neuritic plaque density significantly relates to increased seeding in MF ADNC compared to MF PART. Higher seeding of ADNC is associated with increased levels of select tau PTMs. This suggests a model in which neuritic plaque-associated processes modify ADNC tau seeding specifically in neocortex and contribute to greater cognitive dysfunction observed in late-stage AD versus PART. Brain image created in Biorender. Kraus, A. (2024) https://BioRender.com/s84o442.

translational modification indirectly via inflammatory pathways[45]. Alternately, it is possible that there is a direct but unidentified interaction between tau seeds and Aβ within neuritic plaques. This could suggest that categorizing PART by CERAD neuritic plaque density and not Thal phase may capture a more biologically meaningful patient population; however, this possibility is admittedly speculative and based only on effects on tau modification/seeding. Extensive additional studies would be needed to evaluate the utility of these two possible criteria.

Why Aβ neuritic plaques do not appear to influence hippocampal tau seeding and PTMs is less clear, although it certainly suggests regional differences in Aβ's effects on tau seeding. While we cannot rule out a direct interaction between Aβ and tau that influences tau seeding and PTMs, our data indicate that the ADNC staging criteria of CERAD score and Thal phase do not fully capture an Aβ/tau PTM relationship in the hippocampus. We also cannot rule out that concurrent Aβ-associated and independent processes could contribute to development of tau neuropathology and PTMs in ADNC. Indeed, a synergistic effect of concurrent processes on tau accumulation could account for the well-established observation that younger patients with ADNC, who have greater neocortical Aβ burden, have relatively greater neocortical (versus hippocampal) NFT burden, while older patients with ADNC have a relatively greater hippocampal (versus neocortical) tau NFT burden[18,46].

Our study reports substantial seeding activity in the midfrontal cortex across Braak II-IV PART and ADNC cases and differentiates the diagnoses with estimated seeding doses and select corresponding PTMs prior to significant detection of regional pathology using tau IHC. Importantly, the selected cohort was not only Braak-matched, but had matched tau load determined by quantitative digital histology. Tau seeding doses correlated with antemortem cognitive performance as well as longitudinal decline, demonstrating that tau seeds can mark clinically meaningful processes. Traditional neuropathologic analysis

(i.e. Braak staging) provides an end-stage snapshot of disease processes and cannot definitively predict neuropathological trajectory, necessitating population-based estimates of disease progression. However, measures of seeding activity identify disease-associated tau seeds prior to overt neuropathology. These findings support the potential utility of tau seeding activity as a predictive biomarker that appears to reflect early clinical and neuropathologic decline. Furthermore, this study also shows a strong cross-sectional and longitudinal association between brain tau seeding and both global and domain-specific cognitive dysfunction, indicating the clinical significance of brain seeding activity, including in the absence of NFT pathology. In particular, future work should focus RT-QuIC studies of antemortem biospecimens and biomarkers in conjunction with post-mortem samples to improve clinical prognostication.

Methods

Standard protocol approvals, registrations, and patient consent

This study complies with relevant ethical regulations. The research protocol was reviewed and approved by the human subjects review board at the University of California, San Diego (UCSD). Informed consent was obtained from all patients or their caregivers consistent with California State law. Tau seeds were characterized using deidentified post-mortem brain tissue.

Participants

Participants were individuals followed at the UCSD Shiley-Marcos Alzheimer's Disease Research Center (ADRC) who met neuropathologic criteria for PART (i.e., Braak stage II-IV, low Aβ burden: Thal phase 0-2)[7] or early-stage ADNC (i.e., Braak stage II-IV, high Aβ burden: Thal phase 3-5)[47] at autopsy. The PART cohort included both cases classified as "definite PART" (Thal phase 0) and "possible PART" (Thal phase 1-2). Participants were included in these cohorts without regard to LATE-NC/TDP-43 or cerebrovascular pathology but were excluded if they did

not have sufficient clinical and cognitive data for analysis or if they had a neuropathologic diagnosis of FTLD (FTLD-tau or FTLD-TDP43), Lewy neuropathology in the brainstem, limbic and neocortical regions, or another neuropathologic condition that could result in neurologic impairment (e.g. Creutzfeldt-Jakob disease, multiple sclerosis). The participant selection process was blinded to all clinical and demographic data.

The final PART and ADNC groups did not differ in the presence of concomitant neuropathologies (Table 1). TDP-43 pathology of LATE was present in approximately 30% of individuals in both groups but did not differ in the stage between them ($\chi2 = 1.19$, $p = 0.91$). Hippocampal sclerosis was also equally common in PART and ADNC ($\chi2 = 1.19$, $p = 0.46$). Both groups had a spectrum of severity of microvascular (arteriolosclerosis) and macrovascular (atherosclerosis) disease that did not differ between them ($\chi2 = 0.53$, $p = 0.91$ and $\chi2 = 3.26$, $p = 0.40$, respectively).

Neuropathological evaluation
Autopsy was performed using a previously described protocol[48]. Briefly, the left hemibrain was fixed in 10% buffered formalin for at least 14 days, then 1 cm coronal sections were evaluated grossly, and sections were taken for paraffin-embedding. Hematoxylin and eosin (H&E) was performed on 5 μm sections of middle frontal cortex (Brodmann areas 8/9), rostral superior temporal cortex, inferior parietal cortex, hippocampus (CA1-CA4 and dentate gyrus), entorhinal cortex, basal ganglia, midbrain with substantia nigra, pons with locus coeruleus, and cerebellar cortex with dentate nucleus.

Neuritic plaques, diffuse plaques, and NFTs were identified on either 10 μm 1% Thioflavin-S stained sections using ultraviolet illumination and a 440 μm bandpass excitation filter, or with IHC staining using antibodies to Aβ (Ab69D/E, polyclonal, Edward Koo, 1:1200) and PHF1 tau (Peter Davies, 1:600). CERAD methods were used to estimate neuritic plaque density[49], Thal phase for location of Aβ pathology[50], and Braak stages for NFT pathology[2].

TDP-43 pathology was identified by IHC for total TDP-43 (Proteintech#10782-2-AP polyclonal, 1:12,000) and staged according to LATE-NC consensus guidelines[51] into "amygdala", "hippocampal", or "neocortical" stages.

Clinical and neuropsychological evaluation
Participants had annual standardized clinical, neurological, and neuropsychological evaluations as previously described[52]. Clinical evaluation included review of history with the patient and/or informant, mental status testing, and assessment of functional impairment. Clinical Dementia Rating (CDR) score and sum of its six subdomain scores (i.e., CDR sum of boxes) were computed[53]. Neuropsychological assessment included tests with sufficient data for analysis for *Global Cognition* (Mini-Mental State Exam [MMSE]); *Memory* (Logical Memory Test, CERAD Word List, California Verbal Learning Test (CVLT); and *Executive functions* (modified Wisconsin Card Sorting Test, Trail Making Test Part B, Digit Symbol Substitution Test, Block Design Test).

Consensus clinical diagnoses were made according to published criteria by at least two board-certified neurologists blind to individual cognitive test scores but told whether neuropsychological assessment identified deficits in two or more cognitive domains. Probable or Possible AD or Mild Cognitive Impairment (MCI) was diagnosed according to NINCDS-ADRDA[54] or NIA-AA criteria[55].

Digital histology
6 μm sections from formalin fixed paraffin embedded sections from MF and HP were immunostained for phospho-tau (AT8, Thermofisher MN1020, 1:500, formic acid antigen retrieval) and Aβ (NAB228 1:5000, Thermofisher 37-4200), formic acid antigen retrieval with methods previously published[56]. Briefly, whole slide images of histology slides at 20X magnification were obtained using a Zeiss AxioScan Z1 (Oberkochen Germany,.czi file type). Pixel size of 6.5 μm² (i.e., pixel resolution

of 0.325 μm), camera resolution of 2560 × 2160, and a bit depth of 16 was used. Digital measurements of pathological burdens were derived using the open-source program QuPath (v0.2.0m2 Belfast, Northern Ireland) which calculated percent area occupied (%AO) for tau and Aβ accumulation[57]. Grey matter regions of interest selected by a single trained rater (DGC) were evaluated for all cases using previously validated sampling methods to determine %AO[56–59]. Color deconvolution intensity thresholds were optimized per each staining run by averaging values of red-blue-green color vectors and optimal minimal optical density values visually tuned from five representative slides per staining run (see Supplemental methods). A down sample value of 2 with a gaussian sigma value of 1 was employed for all detections.

Tissue homogenization
Frozen tissue corresponding to the fixed contralateral sections used for histopathology were obtained. It should be noted that both PART and ADNC exhibit asymmetry in the degree of neuropathology, especially in the early stages evaluated for this project[60]. Although it is a widespread practice of brain banks to divide the brain in half for fixation and freezing, this is a known limitation that may attenuate the strength of associations identified. Tissue from multiple locations on each sample were combined while acquiring tissue for homogenization to ensure representative homogenates. 10% w/v brain tissue homogenates were prepared with ice-cold 1X PBS (10 mM sodium phosphate dibasic heptahydrate, 10 mM sodium phosphate monobasic monohydrate, 130 mM NaCl) with 1% v/v phosphatase inhibitor (TFS, 78428) and cOmplete protease inhibitors, EDTA-free (Roche, 1187358001). Homogenization was completed using 1 mm zirconia/silica beads (BioSpec Products) in a BeadMill (Fisher Scientific). Additional high ADNC cases characterized in previous studies[19,61] were used as comparative cases (Supplementary Table 4). Previous experiments have demonstrated no notable differences in seeding activity or immunoreactivity in the absence of phosphatase inhibitor in these assays under conditions used. The homogenates were then chilled on ice for 5 minutes prior to centrifugation at 2000 × g for 2 minutes at 4 °C. The supernatants were then collected, aliquoted for future use, and stored at −80°C.

Tau RT-QuIC assay
K12 RT-QuIC assays (which selectively detect and amplifies 3R/4R and 3R tau seeds) were utilized to determine 3R/4R tau seeding activities based on previously published protocols[28]. Tau knock-out mouse brain homogenate (BH) was used as a negative control for the assay. Seeding doses (SD_{50}s) indicate the dilution at which half of replicate reactions (quadruplicate well analysis) are positive and can be semi-quantitatively estimated using endpoint dilution analysis of RT-QuIC readouts. Endpoint dilution was always reached for SD_{50} calculation. SD_{50}s were calculated as previously described[21] with Spearman-Karber[62] using 10-fold serial dilutions of BH or sarkosyl-insoluble equivalent in diluent buffer (0.526% mouse tau KO BH/N2/10 mM HEPES, pH 7.4). 384-well microplates (TFS, 242764) were seeded with sample dilutions in reaction mixture (6.5 μM K12CFh, 40 μM heparin, 40 mM HEPES, 400 mM NaF, and 10 μM Thioflavin T [ThT]) and sealed (TFS, 232702). The microplates were then incubated at 42 °C with alternate 1-minute cycles of orbital shaking (500 rpm) and rest in a BMG FLUOstar Omega plate reader. ThT fluorescence reads (450-10 nm ex and 480-10 nm em bottom reading) were taken every 45 minutes for a total of 60 hours. The intra-assay coefficient of variation based on 20+ runs of an AD positive control brain tissue homogenate is 5.35%. All initial RT-QuIC experiments and analysis was conducted blinded.

Immunoblotting
Samples were prepared for gel electrophoresis using NuPAGE™ LDS Sample Buffer (4X) (Invitrogen, NP0007) and NuPAGE™ Sample Reducing Agent (10X) (Invitrogen, NP0009) and heated at 70 °C for

10 minutes. Samples were then loaded into NuPAGE™ 10%, Bis-Tris, 1.0–1.5 mm, Mini Protein Gels (Invitrogen, NP0303BOX) and electrophoresed at 200 mV for 20-30 minutes. The gel was then transferred to a PVDF membrane via the Invitrogen™ iBlot™ 2 Gel Transfer Device and subjected to blocking washes and antibody incubations with the Invitrogen™ iBind™ Flex Western Device as also described in previously published protocols[19] with the primary antibodies directed to mid-domain tau (HT7, BT2) and C-terminal tau (D1M9X) epitopes in addition to phospho-tau epitopes (AT8, pThr217) as further described in Supplemental methods. Secondary antibodies (Goat Anti-Rabbit whole IgG PAP pAb, Jackson ImmunoResearch Laboratories, 111-055-144 and Goat Anti-Mouse whole IgG PAP pAb, Jackson ImmunoResearch Laboratories, 111-055-146) were diluted 1:1000 and 1:300, respectively, in iBind™ Solution Kit buffer. The membranes were then developed in AttoPhos® Substrate (Promega, S1011) and imaged on an ImageQuant LAS4000mini (GE).

Quantitation using dot blotting
10% BHs were diluted 1:4 in RIPA buffer (25 mM TrisHCl pH 7.4, 150 mM NaCl, 1% Triton X-100, 1% DOC, 0.1% SDS) and incubated for 30 minutes at 4 °C. PVDF membranes (Bio-Rad, 6120177) were activated in methanol for 30 seconds and equilibrated in TBS (20 mM Tris-HCl pH 7.5, 500 mM NaCl) for 5 minutes. One filter paper (Bio-Rad, 1620161) was wetted in TBS and placed on top of a dry one. The equilibrated PVDF was placed on top of the filter paper stack and 2 µL of sample was spotted on the membrane. After spotting, the membrane was dried at 37 °C for 1 hour and reactivated in methanol and equilibrated in TBS-T (TBS + 0.05% Tween 20). The membrane was then incubated with Ponceau S total protein stain (Cell Signaling Technology, 59803) for 10 minutes, rinsed with water to minimize background and imaged using Canon CanoScan LiDE 300 Scanner 2995C002. Membranes were destained with repeat 5 minute (5-6X) washes of TBS-T prior to antibody incubations which were performed using the methods and antibody incubations described for immunoblotting methods above. Analysis of immunoreactivity was done with three technical replicates of the same BH aliquot using ImageJ software by normalizing the immunostained peak area to the Ponceau S peak area of the same spot.

Sarkosyl-insoluble tau preparation
Preparation of sarkosyl-insoluble (SI) tau followed an adapted protocol used in our prior studies[19]. A bead mill homogenizer was used to make 10% w/v BHs with a homogenization buffer composed of 10 mM Tris-HCl (Sigma, T6066) pH 7.4, 0.8 M NaCl (Sigma, S7653), 1 mM EGTA (Sigma, 4100), and 10% w/v D-sucrose (Fisher, 57-50-1) filter sterilized with a 22 µm filter. Homogenates were centrifuged at 20,000 × g for 20 minutes at 4 °C. Supernatant was collected and the pellet was resuspended in homogenization buffer and re-centrifuged at 20,000 × g for 20 minutes at 4 °C. Supernatants were pooled, 10% v/v of 10% w/v N-Laurylsarcosine (Sigma, L5125) was added, and the solutions were rotated at room temperature for 60 minutes. The solution was centrifuged at 100,000 × g for 60 minutes at 4 °C and the resulting pellet was resuspended with 1X PBS, sonicated for 1 min, and stored at −80°C.

Sarkosyl-insoluble fraction concentration estimation
The concentration of sarkosyl-insoluble (SI) material was determined according to a previously published protocol[19]. Briefly, a standard curve was created with known recombinant protein concentrations (~ 0.02 - 0.2 mg/mL) and ImageJ analysis. The fitted linear regression was used to calculate the protein concentration of SI fractions based on their total protein peak area. The calculated concentrations were used to determine the volume needed to load equivalent material for western blot analysis. The BH equivalence was determined based on the mass of tissue used for isolation and subsequently used for RT-QuIC analysis.

Statistics & reproducibility
Clinical and neuropathologic variables of the PART and ADNC groups were compared using Welch's unequal variance t-test for continuous variables, and Pearson's Chi-squared test (with Yates' continuity correction for 2 × 2 contingency tables). Potential sex effects on histologic tau density, PTMs, and seeding activity were tested using unequal variance t-test. No significant sex-dependent differences were noted as further detailed in Supplementary Table 2. Correlational analyses were performed using Pearson's correlation with R-squared values reported as the proportion of variance explained. The effect of predictors with more than two levels on pathologic outcomes were performed using ANOVA (type II), followed by Tukey's HSD post-hoc test in the case of significant results. The relationship of seeding with PTMs was modeled using linear and logarithmic regression. The logarithmic models universally produced a better fit than the linear models and are reported along with their R-squared values.

Digital histologic measures of the area occupied were natural log-transformed, while SD_{50} values were $\log_{10}$ transformed according to standard practice[19,28]. Cognitive domain Z-scores were created from the neuropsychological test battery using previously described methods[18,63]. As the focus of the analyses was on hippocampal and midfrontal neuropathologic burden, domain scores for *Memory* and *Executive Function* were generated from the selected cognitive tests, described above. The scores were transformed to z-scores using reference values from an independent pool of 61 robust normal controls without neuropathologic confirmation but clinically diagnosed as cognitively normal on their first and all subsequent annual evaluations (average 7.8 ± 6.3 evaluations).

Cross-sectional analyses of the neuropathologic predictors of scores on the MMSE and the cognitive domain scores at the last clinical evaluation were performed using linear regression adjusting for age at death and education. Memory and executive function cognitive domain composites were generated from the UCSD ADRC neuropsychological battery blinded to seeding activity. Longitudinal decline on each of these cognitive measures was examined in the 10 years prior to death using linear mixed effects models adjusting for age at death, and education, along with each of their interactions by time. Participant-specific intercepts and slopes were assumed to follow a normal distribution with unknown variance and were included as random effects.

Reporting summary
Further information on research design is available in the Nature Portfolio Reporting Summary linked to this article.

Data availability
Data supporting the findings of this study are available within the article and Supplementary Information file and available from corresponding authors upon request. Source data are provided with this paper.

References
1. Ziontz, J. et al. Tau pathology in cognitively normal older adults. *Alzheimers Dement (Amst.)* **11**, 637–645 (2019).
2. Braak, H., Alafuzoff, I., Arzberger, T., Kretzschmar, H. & Del Tredici, K. Staging of Alzheimer disease-associated neurofibrillary pathology using paraffin sections and immunocytochemistry. *Acta Neuropathol.* **112**, 389–404 (2006).
3. Braak, H. & Braak, E. Neuropathological stageing of Alzheimer-related changes. *Acta Neuropathol.* **82**, 239–259 (1991).
4. Goedert, M., Eisenberg, D. S. & Crowther, R. A. Propagation of Tau Aggregates and Neurodegeneration. *Annu. Rev. Neurosci.* **40**, 189–210 (2017).
5. Jucker, M. & Walker, L. C. Propagation and spread of pathogenic protein assemblies in neurodegenerative diseases. *Nat. Neurosci.* **21**, 1341–1349 (2018).

6. Shi, Y. et al. Structure-based classification of tauopathies. *Nature* **598**, 359–363 (2021).

7. Crary, J. F. et al. Primary age-related tauopathy (PART): a common pathology associated with human aging. *Acta Neuropathol.* **128**, 755–766 (2014).

8. Jellinger, K. A. et al. PART, a distinct tauopathy, different from classical sporadic Alzheimer disease. *Acta Neuropathol.* **129**, 757–762 (2015).

9. Shi, Y. et al. Cryo-EM structures of tau filaments from Alzheimer's disease with PET ligand APN-1607. *Acta Neuropathol.* **141**, 697–708 (2021).

10. Savola, S. et al. Primary age-related tauopathy in a Finnish population-based study of the oldest old (Vantaa 85+). *Neuropathol. Appl. Neurobiol.* **48**, e12788 (2022).

11. Robinson, J. L. et al. Non-Alzheimer's contributions to dementia and cognitive resilience in The 90+ Study. *Acta Neuropathol.* **136**, 377–388 (2018).

12. Walker, J. M., White, C. L., Farrell, K., Crary, J. F. & Richardson, T. E. Neocortical Neurofibrillary degeneration in primary age-related tauopathy. *J. Neuropathol. Exp. Neurol.* **81**, 146–148 (2022).

13. Bell, W. R. et al. Neuropathologic, genetic, and longitudinal cognitive profiles in primary age-related tauopathy (PART) and Alzheimer's disease. *Alzheimers Dement* **15**, 8–16 (2019).

14. Besser, L. M. et al. Differences in cognitive impairment in primary age-related tauopathy Versus Alzheimer Disease. *J. Neuropathol. Exp. Neurol.* **78**, 219–228 (2019).

15. Teylan, M. et al. Clinical diagnoses among individuals with primary age-related tauopathy versus Alzheimer's neuropathology. *Lab Invest* **99**, 1049–1055 (2019).

16. Bancher, C. & Jellinger, K. A. Neurofibrillary tangle predominant form of senile dementia of Alzheimer type: a rare subtype in very old subjects. *Acta Neuropathol.* **88**, 565–570 (1994).

17. Jellinger, K. A. & Attems, J. Neurofibrillary tangle-predominant dementia: comparison with classical Alzheimer disease. *Acta Neuropathol.* **113**, 107–117 (2007).

18. Smirnov, D. S. et al. Association of neurofibrillary tangle distribution with age at onset-related clinical heterogeneity in alzheimer disease: an autopsy study. *Neurology* **98**, e506–e517 (2022).

19. Manca, M. et al. Tau seeds occur before earliest Alzheimer's changes and are prevalent across neurodegenerative diseases. *Acta Neuropathol.* **146**, 31–50 (2023).

20. Standke, H. G. & Kraus, A. Seed amplification and RT-QuIC assays to investigate protein seed structures and strains. *Cell Tissue Res.* **392**, 323–335 (2023).

21. Kraus, A. et al. Seeding selectivity and ultrasensitive detection of tau aggregate conformers of Alzheimer disease. *Acta Neuropathol.* **137**, 585–598 (2019).

22. Kaufman, S. K., Del Tredici, K., Thomas, T. L., Braak, H. & Diamond, M. I. Tau seeding activity begins in the transentorhinal/entorhinal regions and anticipates phospho-tau pathology in Alzheimer's disease and PART. *Acta Neuropathol.* **136**, 57–67 (2018).

23. Bennett, R. E. et al. Enhanced Tau Aggregation in the Presence of Amyloid beta. *Am. J. Pathol.* **187**, 1601–1612 (2017).

24. Wesseling, H. et al. Tau PTM profiles identify patient heterogeneity and stages of Alzheimer's Disease. *Cell* **183**, 1699–1713.e1613 (2020).

25. Jia, J. et al. Biomarker Changes during 20 Years Preceding Alzheimer's Disease. *N. Engl. J. Med.* **390**, 712–722 (2024).

26. Xia, Y., Prokop, S. & Giasson, B. I. Don't Phos Over Tau": recent developments in clinical biomarkers and therapies targeting tau phosphorylation in Alzheimer's disease and other tauopathies. *Mol. Neurodegen.* **16**, 37 (2021).

27. Moloney, C. M., Lowe, V. J. & Murray, M. E. Visualization of neurofibrillary tangle maturity in Alzheimer's disease: A clinicopathologic perspective for biomarker research. *Alzheimers Dement* **17**, 1554–1574 (2021).

28. Metrick, M. A. et al. A single ultrasensitive assay for detection and discrimination of tau aggregates of Alzheimer and Pick diseases. *Acta Neuropathol. Commun.* **8**, 22 (2020).

29. Nelson, P. T. et al. Clinicopathologic correlations in a large Alzheimer disease center autopsy cohort: neuritic plaques and neurofibrillary tangles "do count" when staging disease severity. *J. Neuropathol. Exp. Neurol.* **66**, 1136–1146 (2007).

30. Ossenkoppele, R. et al. Tau PET patterns mirror clinical and neuroanatomical variability in Alzheimer's disease. *Brain* **139**, 1551–1567 (2016).

31. Ioannou, K. et al. Tau PET positivity predicts clinically relevant cognitive decline driven by Alzheimer's disease compared to comorbid cases; proof of concept in the ADNI study. *Mol Psychiatry* (2024).

32. Arezoumandan, S. et al. Regional distribution and maturation of tau pathology among phenotypic variants of Alzheimer's disease. *Acta Neuropathol.* **144**, 1103–1116 (2022).

33. Ercan, E. et al. A validated antibody panel for the characterization of tau post-translational modifications. *Mol. Neurodegener.* **12**, 87 (2017).

34. Serrano-Pozo, A., Das, S. & Hyman, B. T. APOE and Alzheimer's disease: advances in genetics, pathophysiology, and therapeutic approaches. *Lancet Neurol.* **20**, 68–80 (2021).

35. Basurto-Islas, G. et al. Accumulation of aspartic acid421- and glutamic acid391-cleaved tau in neurofibrillary tangles correlates with progression in Alzheimer disease. *J. Neuropathol. Exp. Neurol.* **67**, 470–483 (2008).

36. Kyalu Ngoie Zola, N. et al. Specific post-translational modifications of soluble tau protein distinguishes Alzheimer's disease and primary tauopathies. *Nat. Commun.* **14**, 3706 (2023).

37. Rosseels, J. et al. Tau monoclonal antibody generation based on humanized yeast models: impact on Tau oligomerization and diagnostics. *J. Biol. Chem.* **290**, 4059–4074 (2015).

38. Block, A. J. & Bartz, J. C. Prion strains: shining new light on old concepts. *Cell Tissue Res.* **392**, 113–133 (2023).

39. Hoyt, F. et al. Cryo-EM structure of anchorless RML prion reveals variations in shared motifs between distinct strains. *Nat. Commun.* **13**, 4005 (2022).

40. Hoyt, F. et al. Cryo-EM of prion strains from the same genotype of host identifies conformational determinants. *PLoS Pathog.* **18**, e1010947 (2022).

41. Manka, S. W. et al. 2.7 A cryo-EM structure of ex vivo RML prion fibrils. *Nat. Commun.* **13**, 4004 (2022).

42. Tarutani, A. et al. Distinct tau folds initiate templated seeding and alter the post-translational modification profile. *Brain* **146**, 4988–4999 (2023).

43. Meisl, G. et al. In vivo rate-determining steps of tau seed accumulation in Alzheimer's disease. *Sci. Adv.* **7**, eabh1448 (2021).

44. Dickson, D. W. et al. Alzheimer's disease. A double-labeling immunohistochemical study of senile plaques. *Am. J. Pathol.* **132**, 86–101 (1988).

45. Tsering, W. & Prokop, S. Neuritic Plaques - Gateways to Understanding Alzheimer's Disease. *Mol. Neurobiol* **61**, 2808–2821 (2023).

46. Murray, M. E. et al. Neuropathologically defined subtypes of Alzheimer's disease with distinct clinical characteristics: a retrospective study. *Lancet Neurol.* **10**, 785–796 (2011).

47. Hyman, B. T. et al. National Institute on Aging-Alzheimer's Association guidelines for the neuropathologic assessment of Alzheimer's disease. *Alzheimers Dement* **8**, 1–13 (2012).

48. Terry, R. D. & Katzman, R. Senile dementia of the Alzheimer type. *Ann. Neurol.* **14**, 497–506 (1983).

49. Mirra, S. S. et al. The Consortium to Establish a Registry for Alzheimer's Disease (CERAD). Part II. Standardization of the neuropathologic assessment of Alzheimer's disease. *Neurology* **41**, 479–486 (1991).

50. Thal, D. R., Rub, U., Orantes, M. & Braak, H. Phases of A beta-deposition in the human brain and its relevance for the development of AD. *Neurology* **58**, 1791–1800 (2002).

51. Nelson, P. T. et al. Limbic-predominant age-related TDP-43 encephalopathy (LATE): consensus working group report. *Brain* **142**, 1503–1527 (2019).

52. Galasko, D. et al. Clinical-neuropathological correlations in Alzheimer's disease and related dementias. *Arch. Neurol.* **51**, 888–895 (1994).

53. Hughes, C. P., Berg, L., Danziger, W. L., Coben, L. A. & Martin, R. L. A new clinical scale for the staging of dementia. *Br. J. Psychiatry* **140**, 566–572 (1982).

54. McKhann, G. et al. Clinical diagnosis of Alzheimer's disease: report of the NINCDS-ADRDA Work Group under the auspices of Department of Health and Human Services Task Force on Alzheimer's Disease. *Neurology* **34**, 939–944 (1984).

55. McKhann, G. M. et al. The diagnosis of dementia due to Alzheimer's disease: recommendations from the National Institute on Aging-Alzheimer's Association workgroups on diagnostic guidelines for Alzheimer's disease. *Alzheimers Dement* **7**, 263–269 (2011).

56. Coughlin, D. G. et al. Digital histological study of neocortical grey and white matter tau burden across tauopathies. *J. Neuropathol. Exp. Neurol.* **81**, 953–964 (2022).

57. Bankhead, P. et al. QuPath: Open source software for digital pathology image analysis. *Sci. Rep.* **7**, 16878 (2017).

58. Coughlin, D. G. et al. Hippocampal subfield pathologic burden in Lewy body diseases vs. Alzheimer's disease. *Neuropathol. Appl. Neurobiol.* **46**, 707–721 (2020).

59. Coughlin, D. et al. Cognitive and pathological influences of tau pathology in lewy body disorders. *Ann. Neurol.* **85**, 259–271 (2019).

60. Walker, J. M. et al. Asymmetry of Hippocampal Tau Pathology in Primary Age-Related Tauopathy and Alzheimer Disease. *J. Neuropathol. Exp. Neurol.* **80**, 436–445 (2021).

61. Coughlin, D. G. et al. Selective tau seeding assays and isoform-specific antibodies define neuroanatomic distribution of progressive supranuclear palsy pathology arising in Alzheimer's disease. *Acta Neuropathol.* **144**, 789–792 (2022).

62. Dougherty, R. M. Animal virus titration techniques. in *Techniques in experimental virology* (ed. Harris, R. J. C.) 183-186 (New York: Academic Press Inc, 1964).

63. Smirnov, D. S. et al. Cognitive decline profiles differ in Parkinson disease dementia and dementia with Lewy bodies. *Neurology* **94**, e2076–e2087 (2020).

64. Kraus, A. Created in BioRender, https://BioRender.com/f48t930 (2024).

Acknowledgements

Author contributions

D.F.B. and D.S.S. contributed equally. A.H. & A.K. conceptualized the study. D.F.B., D.S.S., D.G.C., I.P., H.G.S., A.H., and A.K. designed and executed the experimental plan, and analyzed and interpreted the data. DFB performed RT-QuIC and DFB, IP, and HGS conducted biochemical profiling experiments. D.S.S., D.G.C., A.H. identified cases and evaluated neuropathology. D.G.C., Y.K., A.U., T.A., D.S.S., A.H. procured brain tissue specimens and D.G.C., Y.K., D.P., A.U., T.A., D.S.S., A.H. conducted immunostaining. D.G.C. conducted a digital neuropathology analysis. D.S.S. composed cognitive domain scores and performed statistical analysis. D.F.B., D.S.S., D.C., A.H., and A.K. wrote the initial manuscript draft, and all authors contributed to writing and revising of the manuscript.

Competing interests

A.K. is a co-inventor on patent US11906530B2 and pending application describing seed amplification methods to detect tau seeds. The remaining authors declare no competing interests.

Additional information

Supplementary information The online version contains supplementary material available at https://doi.org/10.1038/s41467-025-56469-7.

Correspondence and requests for materials should be addressed to Annie Hiniker or Allison Kraus.

Peer review information *Nature Communications* thanks Aimee Kao, who co-reviewed with Courtney Lane-Donovanand the other, anonymous, reviewers for their contribution to the peer review of this work. A peer review file is available.

Reprints and permissions information is available at http://www.nature.com/reprints

Publisher's note Springer Nature remains neutral with regard to jurisdictional claims in published maps and institutional affiliations.

[1]Department of Pathology, Case Western Reserve University School of Medicine, Cleveland 44106 OH, USA. [2]Department of Neurosciences, University of California San Diego, La Jolla, CA 92037, USA. [3]Department of Pathology, Harvard Medical School, Mass General Brigham, Boston 02114 MA, USA. [4]Department of Pathology, University of California San Diego, La Jolla 92037 CA, USA. [5]Department of Pathology, University of Southern California Keck School of Medicine, Los Angeles 90033 CA, USA. [6]These authors contributed equally: Danielle F. Browne, Denis S. Smirnov. ✉e-mail: ahiniker@usc.edu; allison.kraus@case.edu